A Static Condensation Reduced Basis Element Approach for the Reynolds Lubrication Equation

Eduard Bader[1,*], Martin A. Grepl[2], and Siegfried Müller[2]

[1] *Aachen Institute for Advanced Study in Computational Engineering Science, RWTH Aachen University, Schinkelstr. 2, 52062 Aachen, Germany.*
[2] *Institut für Geometrie und Praktische Mathematik, RWTH Aachen University, Templergraben 55, 52056 Aachen, Germany.*

Abstract. In this paper, we propose a Static Condensation Reduced Basis Element (SCRBE) approach for the Reynolds Lubrication Equation (RLE). The SCRBE method is a computational tool that allows to efficiently analyze parametrized structures which can be decomposed into a large number of similar components. Here, we extend the methodology to allow for a more general domain decomposition, a typical example being a checkerboard-pattern assembled from similar components. To this end, we extend the formulation and associated *a posteriori* error bound procedure. Our motivation comes from the analysis of the pressure distribution in plain journal bearings governed by the RLE. However, the SCRBE approach presented is not limited to bearings and the RLE, but directly extends to other component-based systems. We show numerical results for plain bearings to demonstrate the validity of the proposed approach.

AMS subject classifications: 76D08, 35J25, 65N30, 65N55

Key words: Reynolds lubrication equation, static condensation, domain decomposition, model order reduction, reduced basis element method, *a posteriori* error estimation.

1 Introduction

The Static Condensation Reduced Basis Element (SCRBE) method was recently introduced in [12] as a computational tool to efficiently analyze parametrized large-scale component-based structures. Such structures — which are composed of a large number of similar or identical parametrized components — naturally appear in many engineering applications. A building, for example, is composed of components like rooms, walls, hallways, and staircases; and each component may be described through parameters like geometry, material constants, and boundary conditions.

The SCRBE method combines two essential ingredients: non-overlapping domain decomposition (resp. substructuring) methods and reduced basis methods. The idea is to employ static condensation to eliminate the internal (to each subdomain resp. component) degrees of freedom

*Corresponding author. *Email addresses:* bader@aices.rwth-aachen.de (E. Bader), grepl@igpm.rwth-aachen.de (M.A. Grepl), mueller@igpm.rwth-aachen.de (S. Müller)

in terms of the corresponding boundary or interface degrees of freedom. Evaluating the entries of the associated Schur Complement System, however, requires numerous evaluations on the subdomain, i.e., bubble solves. If standard discretization techniques like finite elements are used to solve for the bubble functions, this step can be quite expensive — especially if one is interested in analyzing many different parameter combinations. This is were the reduced basis method comes into play.

The reduced basis method [9, 21, 22] is a model order reduction technique which allows efficient and reliable reduced order approximations for a large class of parametrized PDEs and is thus used to approximate the bubble functions. The offline-online computational decomposition allows to move expensive precomputations to the offline stage, the bubble solves are then performed efficiently online. Furthermore, rigorous and efficiently evaluable *a posteriori* bounds have been developed for the system-level error of the SCRBE approximation with respect to the underlying finite element approximation [12]. Within the last two years, the SCRBE method has been extended to also incorporate port reduction [6, 7] and has been successfully extended to treat various engineering problems [11, 13, 23].

We note that the SCRBE method comprises ideas from the Reduced Basis Element (RBE) method [17, 18] and the classical Component Mode Synthesis (CMS) [5, 10]. The RBE method employs the reduced basis method to approximate the bubble functions, but couples the components through a mortar-type procedure. The CMS employs a static condensation to "couple" the components, but uses an eigenmodal expansion to approximate the bubble functions. Indeed, the SCRBE method advantageously combines both approaches: the reduced basis treatment of bubble functions enables parametric variations of the components, whereas component coupling through static condensation enables the derivation of rigorous system-level *a posteriori* error bounds.

In this paper, we employ the SCRBE method to study the pressure distribution within a plain bearing governed by the Reynolds Lubrication equation (RLE). Our main contribution is to extend the SCRBE methodology introduced in [12] to consider a more general domain decomposition. More precisely, in [12] each component is allowed to have at most one neighbor on each port. This assumption excludes the typical wireframe approximation [4], where more than two components "meet" at a junction. Here, we consider a two-dimensional rectangular computational domain, i.e., an unfolded plain bearing, which is decomposed into small rectangular components forming a checkerboard pattern; the interface thus contains junctions where four components meet. The wireframe approximation has implications on the definition of the port degrees of freedom as well as on the *a posteriori* error bound. We show how to extend the work from [12] to this case in the sequel. Furthermore, our second contribution is to present an improved, i.e., sharper, *a posteriori* error bound for the system-level formulation compared to the one proposed in [12]. Although we consider only a two-dimensional domain with a checkerboard pattern in this paper, the derivations presented directly extend also to more general two-dimensional and also three-dimensional wireframe approximations.

This paper is organized as follows. In Section 2 we introduce our specific problem of interest. We briefly explain the physical background, summarize the derivation of the Reynolds Lubrication Equation, derive the parametrized weak formulation, and show results for a model plain bearing. The SCRBE method is discussed in Section 3, where we review the results from [12] and show

the extension to account for the wireframe approximation. In Section 4, we present the *a posteriori* error bound formulation for the more general domain decomposition considered in this paper. Finally, in Section 5 we present numerical results for the model plain bearing introduced in Section 2.

2 The Reynolds Lubrication Equation

2.1 Motivation and Strong Formulation

The motivation for our work is to study the pressure distribution within a plain bearing. Plain bearings are the least expensive and simplest type of bearing and appear in almost all industrial areas. Since they do not contain rolling elements, plain bearings are compact and lightweight and at the same time have a high load-carrying capacity. The load-carrying capacity, however, strongly depends on the pressure distribution within the lubricant. Figure 1(a) shows a sketch of a plain bearing under a hydrodynamic lubrication state, i.e., the journal is rotating. The centerline of the rotating journal is shifted from the bearing centerline resulting in a gap height sketched in Figure 1(b). A lubrication wedge forms, resulting in a pressure build-up carrying the load; we refer to e.g. [3] for a more detailed explanation. Throughout this paper, we assume a hydrodynamic lubrication state with full-film condition, i.e., the load is carried exclusively by the lubricant and there is no contact between the journal and outer bearing surface.

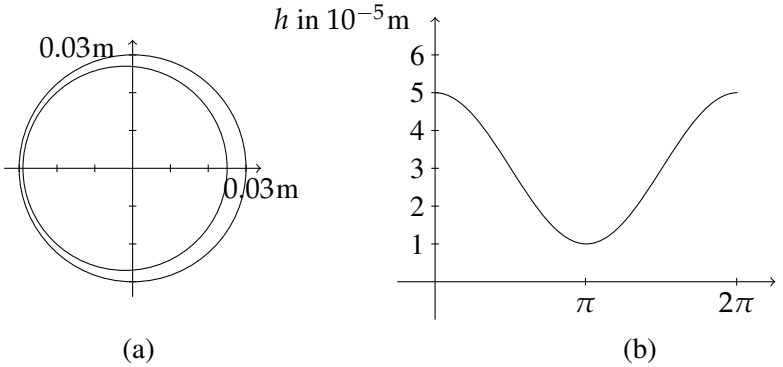

Figure 1: (a) Sketch of journal and outer bearing surface. (b) Gap height as a function of the circumference with maximal eccentricity of $6 \cdot 10^{-5}$ m.

Plain bearings sometimes contain grooves in the bearing surface to help achieve the full-film condition. It has recently also been shown in experiments and simulations [2,8,15,16] that grooves or small dents can not only improve the lubrication properties but also the pressure distribution, thus increasing the lifespan and allowing for a higher load-capacity. The pattern as well as shape and size of the grooves resulting in an optimal pressure distribution, however, are generally not known.

In this paper we consider a specific geometric configuration sketched in Figure 2 to derive the methodology and to subsequently serve as a model problem for the numerical tests. The sketch

shows the unfolded bearing, i.e., cut open on the left and right boundary, the top and bottom boundaries thus correspond to the sides of the bearing. We assume that the bearing surface contains a regular pattern of grooves. To this end, we split the surface into 18×4 equal components, each containing a groove in the middle. The size and depth of the grooves serve as parameters to describe the components. Our goal is to develop a numerical method that allows to efficiently analyze the influence of the grooves on the pressure distribution in the lubricant.

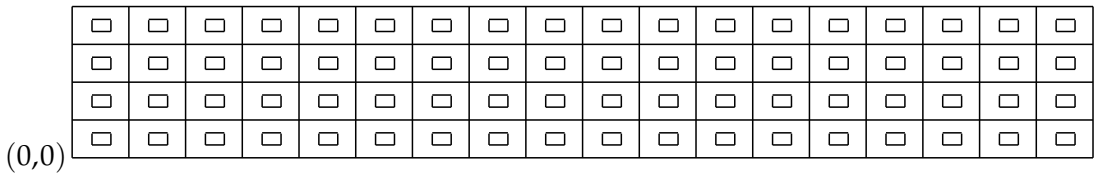

Figure 2: Unfolded outer bearing composed of 18×4 components. The size (m) and depth (m) of the grooves in the middle of each component serve as parameters.

The pressure within the lubricant is governed by the incompressible Navier-Stokes equations

$$\rho\frac{D\mathbf{u}}{Dt}=-\nabla p+\mu_V\Delta\mathbf{u},\quad \operatorname{div}\mathbf{u}=0, \tag{2.1}$$

where ρ is the density, μ_V the dynamic viscosity, p the pressure, $\mathbf{u}\in\mathbb{R}^3$ the velocity, and the material derivative is given by $\frac{D\mathbf{u}}{Dt}\equiv\partial_t\mathbf{u}+u_1\partial_x\mathbf{u}+u_2\partial_y\mathbf{u}+u_3\partial_z\mathbf{u}$. Given the conditions in a plain bearing, however, the Navier-Stokes equations can be simplified considerably to arrive at the Reynolds Lubrication equation [3,20]. To this end, we consider the sketch in Fig. 3 showing a detail of a plain bearing. We denote the distances of the journal and outer bearing to the center by h_1 and h_2 and the corresponding velocities in x-, y-, and z-direction by u_1,u_2, v_1,v_2, and w_1,w_2, respectively. Under certain assumptions — i.e., (i) incompressibility of the lubricant, (ii) constant dynamic viscosity μ_V, (iii) the variation of the height between the bearing parts is small, (iv) the velocities of the lubricant normal to the bearing is much smaller than the one tangential to the bearing, and (v) the pressure is constant in the y-direction — we obtain the RLE [3,20]

$$\nabla\cdot(\frac{\rho h^3}{12\mu_V}\nabla p)=u\partial_x(\rho h)+w\partial_z(\rho h)+\partial_t(\rho h), \tag{2.2}$$

where $p(x,z)$ is the pressure distribution within the lubricant, $\rho(x,z)=\text{const}$ the density of the lubricant, μ_V the dynamic viscosity, $h(x,z)=h_2(x,z)-h_1(x,z)$ the distance in y-direction between the journal and outer bearing, and $u(x,z)=\frac{1}{2}(u_2(x,z)+u_1(x,z))$ and $w(x,z)=\frac{1}{2}(w_2(x,z)+w_1(x,z))$ the average velocities of the lubricant in the x- and z- direction, respectively. Note that the RLE is defined on a two-dimensional domain $\Omega\subset\mathbb{R}^2$, i.e., the unfolded bearing, and we thus impose zero Dirichlet boundary conditions on the sides of the bearing (corresponding to the top and bottom in Figure 2) and periodic boundary conditions where the bearing is cut open (corresponding to the left and right sides in Figure 2).

In a system level simulation of an engine, for example, the RLE is coupled with a Multibody simulation (MBS). The motion of the engine parts, e.g. the crankshaft, are computed from the

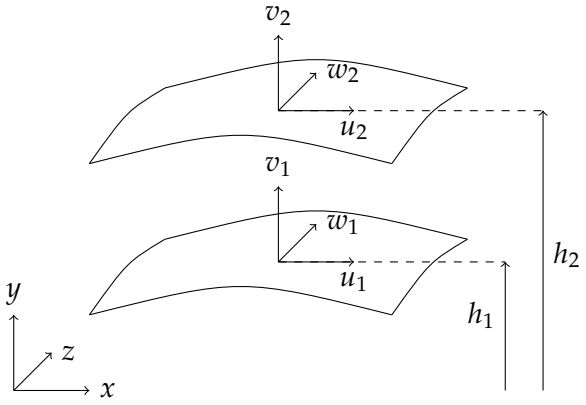

Figure 3: The journal and the outer bearing of the plain bearing with their distances h_1,h_2 to the center. Furthermore, u_1,u_2 are the velocities of the bearing parts in the x-direction, v_1,v_2 are the velocities in the y-direction (height), and w_1,w_2 are the velocities in the z-direction.

MBS, whereas the bearing reactions are computed from the pressure distribution within the bearing governed by the RLE (2.2). In a discrete time simulation setting, the RLE thus needs to be solved at each timestep: The height $h(x,z)$ and velocities $u(x,z)$ and $w(x,z)$ entering (2.2) are considered known inputs from the MBS, the pressure distribution $p(x,z)$ is computed, and the bearing reactions are obtained by integrating the pressure over Ω. The bearing reactions are then applied to the MBS to step forward in time. A single MBS thus requires numerous solutions of the RLE. Furthermore, the optimization of the location and size of the grooves in Figure 2 requires many (optimization) iterations and in turn Mulitbody simulations. Our goal is therefore to develop a methodology which allows to efficiently solve the RLE.

2.2 Weak Formulation

We first introduce the Hilbert space X_e with $H^1_0(\Omega) \subset X_\mathrm{e} \subset H^1(\Omega)$ where $H^1(\Omega) \equiv \{v \mid v \in L^2(\Omega), \nabla v \in (L^2(\Omega))^2\}$, $H^1_0(\Omega) \equiv \{v \mid v \in H^1(\Omega), v|_{\partial\Omega} = 0\}$, and $L^2(\Omega)$ is the space of square integrable functions over Ω, where Ω is our bounded domain in $\mathbb{R}^2$ with Lipschitz continuous boundary $\partial\Omega$.[†] The inner product and induced norm associated with X_e are given by $(\cdot,\cdot)_X$ and $\|\cdot\|_X = \sqrt{(\cdot,\cdot)_X}$, respectively. We assume that the norm $\|\cdot\|_X$ is equivalent to the $H^1(\Omega)$-norm and denote the dual space of X_e by X'_e. Furthermore, let $\mathcal{D} \subset \mathbb{R}^P$ be a prescribed compact parameter set, in which our input parameter $\mu = (\mu_1,\ldots,\mu_P)$ resides.

We directly consider a finite element approximation for the infinite-dimensional problem. To this end, we introduce the piecewise linear conforming finite element space $X \subset X_\mathrm{e}$. We shall assume that the space X is sufficiently rich, resulting in typically large $\mathcal{N} = \dim(X)$, such that the finite element solutions guarantee a desired accuracy over the whole parameter domain $\mathcal{D}$. In the reduced basis literature this is usually referred to as the "truth" approximation. We further recall that the reduced basis approximation shall be built upon – and the reduced basis error thus evaluated with respect to – the truth solution.

We derive the weak formulation of (2.2) by multiplication with a test function $v \in X$, integration

[†]The subscripts "e" denote "exact".

by parts, and invoking the boundary conditions to obtain: $p \in X$ satisfies

$$\tilde{a}(p,v;h) = \tilde{f}(v;h_1,h_2,u_1,u_2,w_1,w_2,v_1,v_2), \quad \forall v \in X, \tag{2.3}$$

where the bilinear and linear forms are given by

$$\tilde{a}(w,v;h) = \int_\Omega \frac{h^3}{12\mu_V} \nabla p \cdot \nabla v \, d\mathbf{x}, \quad \forall w,v \in X \tag{2.4}$$

and

$$\begin{aligned}\tilde{f}(v;h_1,h_2,u_1,u_2,w_1,w_2,v_1,v_2) = &\int_\Omega h\frac{1}{2}(u_1+u_2)\partial_x v + h\frac{1}{2}(w_1+w_2)\partial_z v \, d\mathbf{x} \\ &- \int_\Omega \Big(\big(u_1\partial_x h_1 + w_1\partial_z h_1 - v_1\big) - \big(u_2\partial_x h_2 + w_2\partial_z h_2 - v_2\big) v \, d\mathbf{x} \Big), \quad \forall v \in X,\end{aligned} \tag{2.5}$$

respectively. Note that the density cancels since we consider the full-film condition with ρ constant and that the material derivative of h_1, h_2 is given by

$$\partial_t h_2 - \partial_t h_1 = \big(u_1\partial_x h_1 + w_1\partial_z h_1 - v_1\big) - \big(u_2\partial_x h_2 + w_2\partial_z h_2 - v_2\big). \tag{2.6}$$

We may further simplify (2.3) for our specific problem setting. First, we consider the outer bearing as the reference coordinate system and thus set the velocities $u_2 = v_2 = w_2 = 0$. Second, we assume that the journal rotates but has zero axial or radial velocity; we thus have $v_1 = w_1 = 0$. Third, we note that in the SCRBE approach we never solve (2.3) on the whole domain shown in Figure 2 at once, but only on the components. We thus approximate the gap height as piecewise linear on each component, i.e., we use a piecewise linear interpolation of the gap height shown in Figure 1(b). On each component, we may thus express the gap height as $h = h_0 + h_x x$, where h_0 and h_x are parameters which are different for each component along the circumference. Finally, we need to incorporate the depth of the grooves. The computational domain for one component, Ω_{comp}, including the domain of the groove in the middle, Ω_{gr}, is sketched in Figure 4. We thus introduce h_{gr} such that $h_{\text{gr}} = 0$ on $\Omega_{\text{comp}} \setminus \Omega_{\text{gr}}$ and h_{gr} is equal to the depth of the groove on Ω_{gr}.

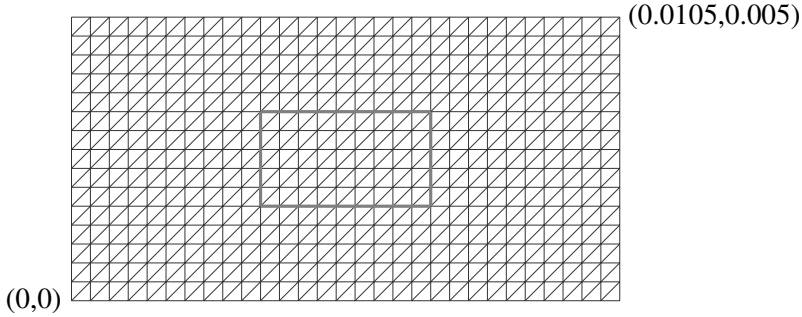

Figure 4: Reference component with triangulation and groove.

The weak formulation (2.3) thus simplifies to: $p \in X$ satisfies

$$a(p,v;\mu) = f(v;\mu), \qquad \forall v \in X, \tag{2.7}$$

where

$$a(w,v;\mu) = \int_\Omega \frac{h^3}{12\mu_V} \nabla w \cdot \nabla v \, d\mathbf{x}, \; \forall w,v \in X \quad \text{and} \quad f(v,\mu) = -\int_\Omega \frac{h}{2} u_1 \partial_x v \, d\mathbf{x}, \; \forall v \in X, \tag{2.8}$$

the gap height is linearly interpolated on each component and given by

$$h(x,z) = h_0 + h_x x + h_{\text{gr}}, \tag{2.9}$$

and the input parameter is defined as $\mu = \{u_1, h_0, h_x, h_{\text{gr}}\} \in \mathcal{D} \subset \mathbb{R}^4$. After expanding $h(x,z)^3$ we observe that the bilinear and linear forms satisfy and affine parameter dependence (see [1] for details) and can be written as

$$a(w,v;\mu) = \sum_{q=1}^{Q_a} \theta_a^q(\mu) a^q(w,v), \qquad \forall w,v \in X \tag{2.10}$$

and

$$f(v;\mu) = \sum_{q=1}^{Q_f} \theta_f^q(\mu) f^q(v), \qquad \forall v \in X \tag{2.11}$$

where the $\theta_{a,f}^q : \mathcal{D} \to \mathbb{R}$ are parameter dependent functions and the $a^q : X \times X \to \mathbb{R}$ and $f^q : X \to \mathbb{R}$ are parameter-independent bilinear and linear forms, respectively.

2.3 Numerical Example

We present a sample solution of the RLE without grooves to explain the general behavior of the solution; the case with grooves is discussed in Section 5. We introduce the domain $\Omega = [0,0.1885\text{m}] \times [0,0.02\text{m}]$, i.e. the bearing has unfolded length 0.1885m and width 0.02m, which is subdivided in 18×4 subdomains; see Fig. 2. We consider the viscosity of the lubricant $\mu_V = 0.01\text{Pa}\cdot\text{s}$ and velocity $u_1 = 4\pi\text{m/s} \approx 12.57\text{m/s}$. As discussed in the last section, we also introduce a piecewise linear interpolation (on each subdomain) of the gap height $h(x) = (30 + 20\cos(\frac{x}{0.1885})) \cdot 10^{-6}$. We thus obtain the pressure distribution sketched in Fig. 5.

We observe that the pressure distribution is point-symmetric and — due to the homogeneous Dirichlet boundary condition — thus also implies a negative pressure and an average pressure over the domain (i.e, integral) of zero. The negative pressure is obviously not physically plausible, since the lubricant cannot carry tensile forces. One option to avoid negative pressures is to consider a bearing under an external pressure, i.e., we apply nonhomogeneous Dirichlet boundary conditions and simply shift the solution upward. In practice, however, the pressure distribution is often "corrected" numerically after the computation in that negative pressures are set to zero and continuity of the pressure gradient is enforced, see e.g. [19]. The details of this correction are beyond the scope of this paper and we therefore consider the original solution in the sequel to derive the SCRBE for the Reynolds Lubrication equation.

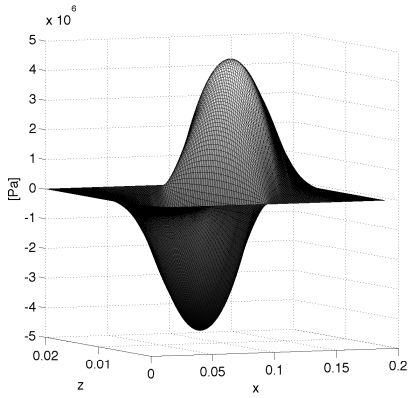

Figure 5: Pressure distribution over the unfolded bearing.

3 Static Condensation Reduced Basis Element Method

We turn to the SCRBE method originally introduced in [12]. Throughout the paper we use the component mode synthesis terminology: "component" refers to a subdomain of the computational domain, "system" to a configuration of components, and "ports" to the areas where components connect. With our application and Figure 2 in mind, we extend the approach presented in [12] to two-dimensional systems where the components are arranged in a checkerboard pattern. Whereas a component is allowed to have at most one neighbor on each port in [12], the checkerboard pattern requires that up to 4 components are connected at ports, i.e., at a crossing-point (see Section 3.1). The extension requires to redefine the port eigenmodes and static condensation (see Section 3.2) and subsequently adapt the *a posteriori* error estimation (see Section 4).

We henceforth consider the following problem defined on a bounded domain Ω with boundary $\partial\Omega$: For a given parameter $\mu \in \mathcal{D}$, find $u(\mu) \in X$ such that

$$a(u(\mu),v;\mu) = f(v;\mu), \qquad \forall v \in X. \tag{3.1}$$

We assume that a is symmetric, continuous, and coercive with respect to the X-norm and that f is linear and bounded. These conditions are obviously satisfied for our model problem defined in (2.7) and (2.8). We next introduce the domain decomposition before discussing the static condensation method and the incorporation of the reduced basis method.

3.1 Domain Decomposition

We assume that the domain Ω can be decomposed into a set $\mathcal{C}_{\mathrm{SYS}}$ of interconnected parametrized components and that each component is associated with a subdomain Ω_i with boundary $\partial\Omega_i$, such that $\overline{\Omega} = \bigcup_{i\in\mathcal{C}_{\mathrm{SYS}}} \overline{\Omega}_i$ with $\Omega_i \cap \Omega_{i'} = \emptyset$, for $i \neq i'$. We denote the restriction of a and f to the subdomains Ω_i by $a_i = a_{|\Omega_i}$ and $f_i = f_{|\Omega_i}$, and note that the parameter vector μ might also be restricted, i.e, $\mu = (\mu_1,\ldots,\mu_I) \in \mathcal{D} = \prod_{i\in\mathcal{C}_{\mathrm{SYS}}} \mathcal{D}_i$.

To simplify the discussion, we consider the specific example sketched in Figure 6: the sample domain shown in Figure 6(a) is decomposed into four equal components shown in Figure 6(b). The sample component in Figure 6(b) contains eight local ports $\mathrm{LP}_i, i = 1,\ldots,8$ which are either

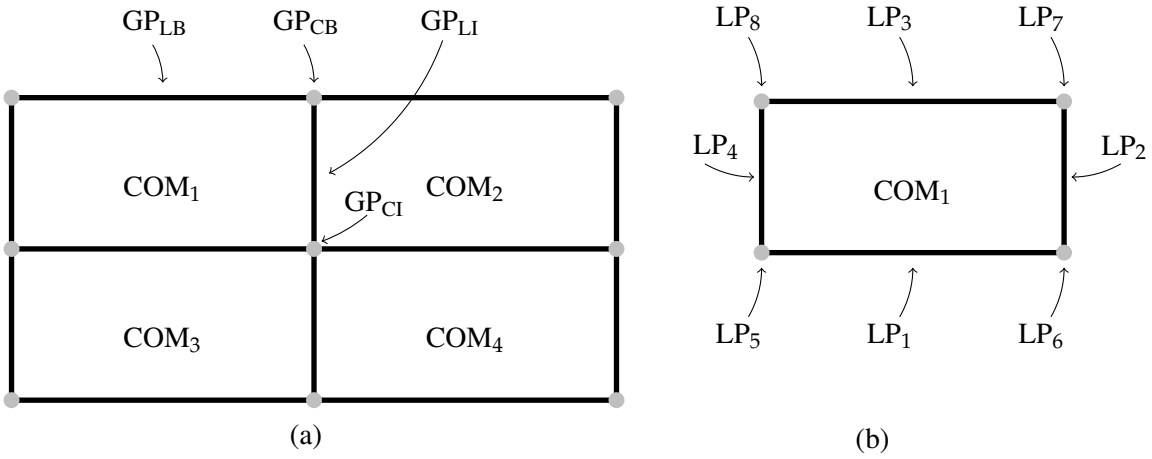

Figure 6: (a) Sample domain $\Omega \subset \mathbb{R}^2$ decomposed into four equal rectangular components, showing four kinds of global ports: 4 $\mathrm{GP}_{\mathrm{LI}}$, 8 $\mathrm{GP}_{\mathrm{LB}}$, 1 $\mathrm{GP}_{\mathrm{CI}}$, 8 $\mathrm{GP}_{\mathrm{CB}}$. (b) A local component with 8 local ports (LP), 4 lines LPs and 4 point LPs.

a line or a (corner) point. We denote the set of LPs on a component by $\mathcal{P}_{\mathrm{COM}}$ and the number of LPs on component i by n_i^{LP}. In the sequel, the distinction between line LPs ($\mathrm{LP}_1,\ldots,\mathrm{LP}_4$) and point LPs ($\mathrm{LP}_5,\ldots,\mathrm{LP}_8$) will be important. We thus also introduce the set of line LPs and corner LPs denoted by $\mathcal{P}^l_{\mathrm{COM}}$ and $\mathcal{P}^c_{\mathrm{COM}}$, respectively; note that $\mathcal{P}_{\mathrm{COM}} = \mathcal{P}^l_{\mathrm{COM}} \cup \mathcal{P}^c_{\mathrm{COM}}$. We denote the portion $\partial\Omega_i$ associated to a specific LP by Γ_{LP}, for a line LP we denote the (closed) domain including the two neighboring point LPs by $\overline{\Gamma}_{\mathrm{LP}}$, e.g., $\overline{\Gamma}_{\mathrm{LP}_1}$ contains the two corner points LP_5 and LP_6. Each local port is associated to a unique global port $\mathrm{GP} \in \mathcal{P}_{\mathrm{SYS}}$ of the same kind, i.e., line to line and point to point. We therefore introduce the mapping π which maps a specific LP of component i to a GP, $\pi : \mathcal{P}_{\mathrm{COM}} \times \mathcal{C}_{\mathrm{SYS}} \to \mathcal{P}_{\mathrm{SYS}}$, $\pi(\mathrm{LP}, i) = \mathrm{GP}$, as well as the pseudo inverse map π_i^{-1} which maps a GP to a LP on component i. We denote by $\mathcal{P}_{\mathrm{SYS}}$ the set and by n_{GP} the number of global ports which have no intersection with the homogeneous Dirichlet boundary conditions of the system. In Figure 6(a) we may distinguish four different GPs: (i) a line GP lying in the interior of the domain Ω, denoted by $\mathrm{GP}_{\mathrm{LI}}$; (ii) a line GP lying on the boundary $\partial\Omega$, denoted by $\mathrm{GP}_{\mathrm{LB}}$; (iii) a point GP lying in the interior of Ω, denoted by $\mathrm{GP}_{\mathrm{CI}}$; and (iv) a point GP lying on the boundary $\partial\Omega$, denoted by $\mathrm{GP}_{\mathrm{CB}}$; in total, the system sketched in Figure 6(a) has 21 GPs. As opposed to the framework introduced in [12], we observe that a component may have up to three neighbors on a point GP. We denote the domain associated to a specific GP by Γ_{GP} and — following the notation for the LPs — we use $\overline{\Gamma}_{\mathrm{GP}}$ for a line GP including the two neighboring points.

We present a simple example with only 4 components to illustrate the above concepts. In Figure 7 we sketch an unfolded bearing consisting of only 4 components with homogeneous Dirichlet conditions on the top and bottom boundaries and periodic boundary conditions on the

left and right boundary. The global ports on the Dirichlet boundary are marked with a dashed line, the components and global ports are numbered in consecutive order. Note that the global ports on the left and right boundary coincide because of the periodic boundary condition. Overall we thus have: 6 $\mathrm{GP}_{\mathrm{LI}}$, 0 $\mathrm{GP}_{\mathrm{LB}}$, 2 $\mathrm{GP}_{\mathrm{CI}}$, 0 $\mathrm{GP}_{\mathrm{CB}}$. In Table 1 we show the corresponding map $\pi : \mathcal{P}_{\mathrm{COM}} \times \mathcal{C}_{\mathrm{SYS}} \to \mathcal{P}_{\mathrm{SYS}}$, $\pi(\mathrm{LP},i) = \mathrm{GP}$ from the sample component shown in Figure 6(b) to the system level configuration in Figure 7.

(LP,i)	GP	(LP,i)	GP	(LP,i)	GP	(LP,i)	GP
1,1	1	1,2	6	1,3	–	1,4	–
2,1	2	2,2	3	2,3	7	2,4	8
3,1	–	3,2	–	3,3	1	3,4	6
4,1	3	4,2	2	4,3	8	4,4	7
5,1	4	5,2	5	5,3	–	5,4	–
6,1	5	6,2	4	6,3	–	6,4	–
7,1	–	7,2	–	7,3	5	7,4	4
8,1	–	8,2	–	8,3	4	8,4	5

Table 1: Mapping $\pi(\mathrm{LP},i) = \mathrm{GP}$ for configuration in Fig. 7 with 4 components and 8 GPs. Note that some LPs are mapped to a GP with homogeneous Dirichlet boundary conditions, which is denoted by $-$.

We next recall the finite element approximation space X of dimension $\dim(X) = \mathcal{N}$. We assume that the triangulation over X honors the decomposition into components defined above. To this end, we define (i) the restriction of functions in X to the ith component as X_i; (ii) the restriction to the ith component with homogeneous Dirichlet boundary conditions on each Γ_{LP}, $\mathrm{LP} \in \mathcal{P}_{\mathrm{COM}}$, by $X_{i,0}$; and (iii) the restriction to a global port as $X(\overline{\Gamma}_{\mathrm{GP}})$, which — in the case of a line GP — contains also the neighboring point GPs, whereas $X(\Gamma_{\mathrm{GP}})$ denotes the restriction to GP without the neighboring points. In the case of a point GP, $X(\overline{\Gamma}_{\mathrm{GP}})$ simply represents the single node of the triangulation lying on GP. Finally, we denote the degrees of freedom on a GP by $\mathcal{N}_{\mathrm{GP}} = \dim(X(\Gamma_{\mathrm{GP}}))$[‡]; for a point GP we thus simply have $\mathcal{N}_{\mathrm{GP}} = 1$. Finally, considering a specific component i with n_i^{LP} local ports, we denote the overall number of degrees of freedom by $\mathcal{N}_i^{\mathrm{LP}}$.

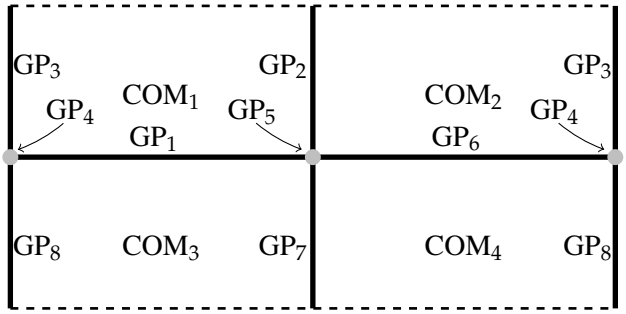

Figure 7: All global ports in a simple configuration with homogeneous conditions at top/bottom (dashed) and a periodic conditions left/right.

Although we restrict our attention to two-dimensional domains and the specific decomposition

[‡]Note that for a line GP with two neighboring points we have $\mathcal{N}_{\mathrm{GP}} = \dim(X(\Gamma_{\mathrm{GP}})) = \dim(X(\overline{\Gamma}_{\mathrm{GP}})) - 2$, i.e. we do not include the two boundary points into the count for the degrees of freedom

sketched in Figure 6(a), the approach also extends for example to three-dimensional domains composed out of cuboids.

3.2 Static Condensation

3.2.1 Eigenmodes

Following [12], we express the degrees of freedom on Γ_{GP} in terms of an eigenfunction expansion. However, given the more general domain decomposition introduced above, we need to adjust the definitions of the eigenfunctions and their harmonic extension to our setting. Furthermore, we need to strictly distinguish between point and line ports. We start with the latter: introduce a basis for the line ports, where the basis functions consist of the complete set of eigenvectors, $\{\chi_k \in X_0(\overline{\Gamma}_{\mathrm{GP}}) : 1 \le k \le \mathcal{N}_{\mathrm{GP}}\}$, where $X_0(\overline{\Gamma}_{\mathrm{GP}}) = \{v \in X(\overline{\Gamma}_{\mathrm{GP}}); v_{|\partial\overline{\Gamma}_{\mathrm{GP}}} = 0\}$, associated with the generalized eigenvalue problem

$$\int_{\overline{\Gamma}_{\mathrm{GP}}} \nabla\chi_k \cdot \nabla v = \lambda_k \int_{\overline{\Gamma}_{\mathrm{GP}}} \chi_{\mathrm{GP},k} v, \qquad \forall v \in X_0(\overline{\Gamma}_{\mathrm{GP}}), \tag{3.2}$$

with $\|\chi_k\|_{L^2(\overline{\Gamma}_{\mathrm{GP}})} = 1$, and the $\lambda_k \in \mathbb{R}$ denote the real positive eigenvalues. We elliptically lift these line port eigenmodes to the interior of neighboring components to obtain a set of interface functions $\Psi_{\mathrm{GP},k}$, $k = 1,\ldots,\mathcal{N}_{\mathrm{GP}}$. Note that $\Psi_{\mathrm{GP},k}$ has support only over the (at most) two components, which connect at the line GP and is zero on all other components. We denote the restriction of $\Psi_{\mathrm{GP},k}$ to a neighboring component i by $\psi_{\mathrm{LP},i,k} \in X_i$, which is computed from

$$\int_{\Omega_i} \nabla\psi_{\mathrm{LP},i,k} \cdot \nabla v = 0, \qquad \forall v \in X_{i;0}, \tag{3.3}$$

$$\psi_{\mathrm{LP},i,k} = \chi_k, \quad \text{on } \Gamma_{\mathrm{LP}} \tag{3.4}$$

$$\psi_{\mathrm{LP},i,k} = 0, \quad \text{on } \Gamma_{\mathrm{LP}'},\ \mathrm{LP}' \in \mathcal{P}_{\mathrm{COM}} \backslash \mathrm{LP}. \tag{3.5}$$

Note that — thanks to the definition of the port basis functions χ_k with homogeneous Dirichlet boundary conditions on the line GP — we obtain consistent boundary conditions for $\psi_{\mathrm{LP},i,k}$ on Ω_i. I.e, $\psi_{\mathrm{LP},i,k}$ is equal to χ_k on Γ_{LP} and zero on all other LPs.

For the point GPs, we simply define "global" piecewise-linear hat functions, which are defined on the wireframe, i.e., we set $\Psi_{\mathrm{GP}} = 1$ at the corresponding GP and to zero at the neighboring point GPs. In Figure 6(a) this would correspond to setting (say) $\Psi_{\mathrm{GP}} = 1$ on $\mathrm{GP}_{\mathrm{CI}}$ and to zero on the eight point GPs on the boundary. The interface function for a point GP thus has support on up to four components.

3.2.2 Bubble Functions and Schur Complement System

Given the definition of the interface functions, we can follow the approach presented in [12] to define the bubble functions and subsequently set up the Schur Complement System (SCS). We express the truth solution of (3.1) in terms of bubble and interface functions as

$$u(\mu) = \sum_{i \in \mathcal{C}_{\mathrm{SYS}}} b_i(\mu) + \sum_{\mathrm{GP} \in \mathcal{P}_{\mathrm{SYS}}} \sum_{k=1}^{\mathcal{N}_{\mathrm{GP}}} \mathbb{U}_{\mathrm{GP},k}(\mu) \Psi_{\mathrm{GP},k} \tag{3.6}$$

where $b_i(\mu) \in X_{i;0}$ for each $i \in \mathcal{C}_{\rm SYS}$, and the $\mathbb{U}_{{\rm GP},k}(\mu)$ with $1 \le k \le \mathcal{N}_{\rm GP}$ and ${\rm GP} \in \mathcal{P}_{\rm SYS}$ are the coefficients of the interface functions. We like to stress that the bubble functions live in the truth finite element space and that the number of coefficients on one global port is equal to the number of degrees of freedom on this particular port. We next insert (3.6) into (3.1) and test on the bubble space of component i, $X_{i;0}$, to obtain

$$a_i\left(b_i(\mu) + \sum_{{\rm LP}\in\mathcal{P}_{\rm COM}} \sum_{k=1}^{n_{\pi({\rm LP},i)}} \mathbb{U}_{\pi({\rm LP},i),k}(\mu)\psi_{{\rm LP},i,k}, v;\mu\right) = f_i(v;\mu), \qquad \forall v \in X_{i;0}. \tag{3.7}$$

It follows from linearity and superposition that we can express $b_i(\mu)$ as

$$b_i(\mu) = b_{i,f}(\mu) + \sum_{{\rm LP}\in\mathcal{P}_{\rm COM}} \sum_{k=1}^{n_{\pi({\rm LP},i)}} \mathbb{U}_{\pi({\rm LP},i),k}(\mu) b_{{\rm LP},i,k}(\mu), \tag{3.8}$$

where $b_{i,f}(\mu) \in X_{i;0}$ satisfies

$$a_i(b_{i,f}(\mu), v;\mu) = f_i(v;\mu), \qquad \forall v \in X_{i;0}, \tag{3.9}$$

and $b_{{\rm LP},i,k}(\mu) \in X_{i;0}$, defined by $\mathcal{N}_i^{\rm LP}$ subproblems, satisfies

$$a_i(b_{{\rm LP},i,k}(\mu), v;\mu) = -a_i(\psi_{{\rm LP},i,k}, v;\mu), \qquad \forall v \in X_{i;0}. \tag{3.10}$$

We note that the previous three equations are well-posed, since the bilinear form a restricted to component i is coercive and continuous on $X_{i;0}$ due to the homogeneous Dirichlet boundary conditions. Plugging (3.8) into (3.6) we obtain

$$u(\mu) = \sum_{i\in\mathcal{C}_{\rm SYS}} b_{i,f}(\mu) + \sum_{{\rm GP}\in\mathcal{P}_{\rm SYS}} \sum_{k=1}^{\mathcal{N}_{\rm GP}} \mathbb{U}_{{\rm GP},k}(\mu)\Phi_{{\rm GP},k}(\mu), \tag{3.11}$$

where

$$\Phi_{{\rm GP},k}(\mu) = \Psi_{{\rm GP},k} + \sum_{i\in\omega_{\rm GP}} b_{\pi_i^{-1}({\rm GP}),k}(\mu), \tag{3.12}$$

and $\omega_{\rm GP}$ denotes the components over which $\Psi_{\rm GP}$ has support. Defining the "skeleton space", $X_{\mathcal{S}}(\mu) \equiv {\rm span}\{\Phi_{{\rm GP},k}(\mu)\colon 1 \le k \le \mathcal{N}_{\rm GP},\ \forall {\rm GP} \in \mathcal{P}_{\rm SYS}\}$, inserting (3.11) into (3.1), and testing with functions in $X_{\mathcal{S}}$ we finally obtain the SCS

$$\sum_{{\rm GP}\in\mathcal{P}_{\rm SYS}} \sum_{k=1}^{\mathcal{N}_{\rm GP}} \mathbb{U}_{{\rm GP},k}(\mu) a(\Phi_{{\rm GP},k}(\mu), v;\mu) = f(v;\mu) - \sum_{i\in\mathcal{C}_{\rm SYS}} a(b_{i,f}(\mu), v;\mu), \quad v \in X_{\mathcal{S}}(\mu). \tag{3.13}$$

Since the computation of the truth quantities $b_{i,f}(\mu) \in X_{i;0}$ from (3.9) and $b_{{\rm LP},i,k}(\mu) \in X_{i;0}$ from (3.10) has to be performed for every new parameter μ, we follow [12] and introduce associated reduced basis approximations. To this end, we introduce reduced basis spaces $\tilde{X}_{f,i;0}$ and $\tilde{X}_{{\rm LP},i,k;0}$

for the bubble functions that are constructed using a Greedy procedure [24]. We then define the reduced basis approximation $\tilde{b}_{i,f} \in \tilde{X}_{f,i;0}$ to $b_{i,f}(\mu)$ such that

$$a_i(\tilde{b}_{i,f}(\mu), v; \mu) = f_i(v; \mu), \qquad \forall v \in \tilde{X}_{f,i;0}, \tag{3.14}$$

and the reduced basis approximation $\tilde{b}_{\mathrm{LP},i,k}(\mu) \in X_{\mathrm{LP},i,k;0}$ to $b_{\mathrm{LP},i,k}(\mu)$ such that

$$a_i(\tilde{b}_{\mathrm{LP},i,k}(\mu), v; \mu) = -a_i(\psi_{\mathrm{LP},i,k}, v; \mu), \qquad \forall v \in \tilde{X}_{\mathrm{LP},i,k;0}. \tag{3.15}$$

Following the same steps as above and appropriately replacing the truth quantities by their reduced basis counterparts, we define a reduced basis "skeleton space", $\tilde{X}_{\mathcal{S}}(\mu) \equiv \mathrm{span}\{\tilde{\Phi}_{\mathrm{GP},k}(\mu) \colon 1 \le k \le \mathcal{N}_{\mathrm{GP}},\ \forall \mathrm{GP} \in \mathcal{P}_{\mathrm{SYS}}\}$, to obtain the reduced basis SCS

$$\sum_{\mathrm{GP} \in \mathcal{P}_{\mathrm{SYS}}} \sum_{k=1}^{\mathcal{N}_{\mathrm{GP}}} \tilde{\mathbb{U}}_{\mathrm{GP},k}(\mu)\, a(\tilde{\Phi}_{\mathrm{GP},k}(\mu), v; \mu) = f(v; \mu) - \sum_{i \in \mathcal{C}_{\mathrm{SYS}}} a(\tilde{b}_{i,f}(\mu), v; \mu), \quad v \in \tilde{X}_{\mathcal{S}}(\mu). \tag{3.16}$$

We note that the number of coefficients $\tilde{\mathbb{U}}_{\mathrm{GP},k}(\mu)$ with $1 \le k \le \mathcal{N}_{\mathrm{GP}}$ and $\mathrm{GP} \in \mathcal{P}_{\mathrm{SYS}}$ and thus the degrees of freedom of the reduced basis SCS is equivalent to the number of coefficients of the (original) truth system (3.13). However, replacing the truth bubble functions with their reduced basis approximations allows to invoke an offline-online decomposition and thus an online-efficient procedure to assemble (3.16). For the well-posedness of (3.16) we refer the reader to [12].

3.2.3 Computational Procedure

We choose $\tilde{\Phi}_{\mathrm{GP}',k'}$, $1 \le k' \le \mathcal{N}_{\mathrm{GP}}$ and $\mathrm{GP}' \in \mathcal{P}_{\mathrm{SYS}}$, as test functions in (3.16) to obtain the linear algebraic system

$$\tilde{\mathbb{A}}(\mu)\tilde{\mathbb{U}}(\mu) = \tilde{\mathbb{F}}(\mu) \tag{3.17}$$

of size $n_{\mathrm{sc}} \equiv \sum_{\mathrm{GP} \in \mathcal{P}_{\mathrm{SYS}}} \mathcal{N}_{\mathrm{GP}}$, where $\tilde{\mathbb{U}}(\mu) \in \mathbb{R}^{n_{\mathrm{sc}}}$ is the vector of coefficients $\tilde{\mathbb{U}}_{k,\mathrm{GP}}(\mu)$, the matrix $\tilde{\mathbb{A}}(\mu) \in \mathbb{R}^{n_{\mathrm{sc}} \times n_{\mathrm{sc}}}$ has entries $\tilde{\mathbb{A}}_{(\mathrm{GP}',k'),(\mathrm{GP},k)}(\mu) \equiv a(\tilde{\Phi}_{\mathrm{GP}',k'}(\mu), \tilde{\Phi}_{\mathrm{GP},k}(\mu); \mu)$, $1 \le k, k' \le \mathcal{N}_{\mathrm{GP}}$, $\mathrm{GP}, \mathrm{GP}' \in \mathcal{P}_{\mathrm{SYS}}$, and the right-hand side $\tilde{\mathbb{F}}(\mu) \in \mathbb{R}^{n_{\mathrm{sc}}}$ has entries $\tilde{\mathbb{F}}_{\mathrm{GP}',k'}(\mu) \equiv f(\tilde{\Phi}_{\mathrm{GP}',k'}; \mu) - \sum_{i \in \mathcal{C}_{\mathrm{SYS}}} a(b_{i,f}(\mu), \tilde{\Phi}_{\mathrm{GP}',k'}; \mu)$, $1 \le k' \le \mathcal{N}_{\mathrm{GP}}$, $\mathrm{GP}' \in \mathcal{P}_{\mathrm{SYS}}$.

The matrix $\tilde{\mathbb{A}}(\mu)$ and vector $\tilde{\mathbb{F}}(\mu)$ can be assembled using a local to global mapping. To this end, we introduce a "local stiffness matrix" $\tilde{\mathbb{A}}^i \in \mathbb{R}^{\mathcal{N}_i^{\mathrm{LP}} \times \mathcal{N}_i^{\mathrm{LP}}}$ and a "local load vector" $\tilde{\mathbb{F}}^i \in \mathbb{R}^{\mathcal{N}_i^{\mathrm{LP}}}$ for component i given by

$$\begin{aligned}
\tilde{\mathbb{A}}^i_{(k',\mathrm{LP}'),(k,\mathrm{LP})}(\mu) &\equiv a_i(\psi_{\mathrm{LP},i,k} + \tilde{b}_{\mathrm{LP},i,k}, \psi_{\mathrm{LP}',i,k'} + \tilde{b}_{\mathrm{LP}',i,k'}; \mu), \\
\tilde{\mathbb{F}}^i_{k',\mathrm{LP}'}(\mu) &\equiv f_i(\psi_{\mathrm{LP}',i,k'} + \tilde{b}_{\mathrm{LP}',i,k'}; \mu) - a_i(\tilde{b}_{i,f}(\mu), \psi_{\mathrm{LP}',i,k'} + \tilde{b}_{\mathrm{LP}',i,k'}; \mu),
\end{aligned}$$

for $1 \le k \le n_{\pi(\mathrm{LP},i)}$, $\forall \mathrm{LP} \in \mathcal{C}_{\mathrm{SYS}}$, and $1 \le k' \le n_{\pi(\mathrm{LP}',i)}$, $\forall \mathrm{LP}' \in \mathcal{C}_{\mathrm{SYS}}$. The assembly then follows directly from the local to global mapping $\mathrm{GP} = \pi(\mathrm{LP}, i)$.

4 A Posteriori Error Estimation

We next turn to the *a posteriori* error estimation. The goal of this section is to derive a bound for the error $\mathbb{U}(\mu)-\tilde{\mathbb{U}}(\mu)$, i.e., between the solution of the reduced basis SCS (3.16) and the truth SCS (3.13). The derivation is based on the results in [12]. Our contribution is to extend the methodology to the more general domain decomposition introduced above.

4.1 Preliminaries

The error in the reduced SCS is due to the reduced basis approximation of the bubble functions. We therefore introduce the residuals $r_{f,i}(\cdot;\mu): X_{i;0} \to \mathbb{R}$ given by

$$r_{f,i}(v;\mu) \equiv f_i(v;\mu) - a_i(\tilde{b}_{i,f}(\mu), v;\mu), \qquad \forall v \in X_{i;0}, \tag{4.1}$$

and $r_{\mathrm{LP},i,k}(\cdot;\mu): X_{i;0} \to \mathbb{R}$, $1 \le k \le n_{\pi(\mathrm{LP},i)}$, $\mathrm{LP} \in \mathcal{P}_{\mathrm{COM}}$, given by

$$r_{\mathrm{LP},i,k}(v;\mu) \equiv -a_i(\psi_{\mathrm{LP},i,k} + \tilde{b}_{\mathrm{LP},i,k}(\mu), v;\mu), \qquad \forall v \in X_{i;0}. \tag{4.2}$$

It then follows from the standard reduced basis *a posteriori* error bounds (see e.g. [21]) that the error between $b_{i,f}(\mu)$ from (3.9) and its reduced basis approximation $\tilde{b}_{i,f}(\mu)$ given by (3.14) satisfies

$$\|b_{i,f}(\mu) - \tilde{b}_{i,f}(\mu)\|_{X_i} \le \frac{\|r_{f,i}(\cdot;\mu)\|_{X'}}{\alpha_i^{\mathrm{LB}}(\mu)}, \tag{4.3}$$

where $\|r_{f,i}(\cdot;\mu)\|_{X'}$ is the dual norm of the residual (4.1) and $\alpha_i^{\mathrm{LB}}(\mu)$ is a lower bound of the coercivity constant, $\alpha_i(\mu) \equiv \inf_{v \in X_{i;0}} \frac{a_i(v,v;\mu)}{\|v\|_{X_i}^2}$, such that $0 < \alpha_i^{\mathrm{LB}}(\mu) \le \alpha_i(\mu)$, $\forall \mu \in \mathcal{D}$. The coercivity lower bound can be computed using the Successive Constraint Method [14]. Furthermore, the error between $b_{\mathrm{LP},i,k}(\mu)$ from (3.10) and its reduced basis approximation $\tilde{b}_{\mathrm{LP},i,k}(\mu)$ given by (3.15) satisfies

$$\|b_{k_i}(\mu) - \tilde{b}_{k_i}(\mu)\|_{X_i} \le \frac{\|r_{\mathrm{LP},i,k}(\cdot;\mu)\|_{X_i'}}{\alpha_i^{\mathrm{LB}}(\mu)}, \tag{4.4}$$

where $\|r_{\mathrm{LP},i,k}(\cdot;\mu)\|_{X_i'}$ is the dual norm of the residual (4.2). For notational convenience, we define the associated energy norm bounds by

$$\Delta_{f,i}(\mu) \equiv \frac{\|r_{f,i}(\cdot;\mu)\|_{X'}}{\sqrt{\alpha_i^{\mathrm{LB}}(\mu)}} \qquad \text{and} \qquad \Delta_{\mathrm{LP},i,k}(\mu) \equiv \frac{\|r_{\mathrm{LP},i,k}(\cdot;\mu)\|_{X_i'}}{\sqrt{\alpha_i^{\mathrm{LB}}(\mu)}}. \tag{4.5}$$

It then follows that the error in a single entry of the local stiffness matrix for a specific component i is bounded by

$$|\mathbb{A}^i_{(\mathrm{LP}',k'),(\mathrm{LP},k)}(\mu) - \tilde{\mathbb{A}}^i_{(\mathrm{LP}',k'),(\mathrm{LP},k)}(\mu)| \le \Delta_{\mathrm{LP},i,k}(\mu) \cdot \Delta_{\mathrm{LP}',i,k'}(\mu), \tag{4.6}$$

and the error of the local stiffness matrix measured in the Frobenius norm, $\|\cdot\|_F$, thus satisfies

$$\|\mathbb{A}^i(\mu)-\tilde{\mathbb{A}}^i(\mu)\|_F^2 \leq \sum_{\mathrm{LP}\in\mathcal{P}_{\mathrm{COM}}} \sum_{k=1}^{n_{\pi(\mathrm{LP},i)}} \sum_{\mathrm{LP}'\in\mathcal{P}_{\mathrm{COM}}} \sum_{k'=1}^{n_{\pi(\mathrm{LP}',i)}} \left(\Delta_{\mathrm{LP},i,k}(\mu)\Delta_{\mathrm{LP}',i,k'}(\mu)\right)^2$$
$$= \left(\sum_{\mathrm{LP}\in\mathcal{P}_{\mathrm{COM}}} \sum_{k=1}^{n_{\pi(\mathrm{LP},i)}} \Delta_{\mathrm{LP},i,k}(\mu)^2\right)^2. \tag{4.7}$$

We refer the reader to [12] for the proof.

4.2 SCS Error Bound

We first consider the error in the statically condensed system matrix. The n_{sc} system level degrees of freedom each correspond to a specific interface degree of freedom k, $1\leq k\leq \mathcal{N}_{\mathrm{GP}}$, i.e., interface function, on a global port GP, $\mathrm{GP}\in\mathcal{P}_{\mathrm{SYS}}$. Given the inverse map $(\mathrm{LP},i)=\pi_i^{-1}(\mathrm{GP})$ defined previously, which maps a global port to a LP on component i, we can thus associate each system level degree of freedom to a local port degree of freedom of a component, i.e., $(\mathrm{GP},k)\rightarrow(\pi_i^{-1}(\mathrm{GP}),k)=(\mathrm{LP},i,k)$, where we assume a consistent numbering of the interface functions on the GPs and LPs. We note, however, that a global port can map onto up to four LPs on four components. To obtain a bound for the (global) SCS matrix, we thus need to keep track of how many LPs and thus components are "connected" at each GP in order to correctly sum up their contributions.

To this end, we define the error in the SCS matrix, $E(\mu)=\mathbb{A}(\mu)-\tilde{\mathbb{A}}(\mu)$, with entries $E_{\ell,\ell'}(\mu)$, $1\leq\ell,\ell'\leq n_{\mathrm{sc}}$. The goal in this section is to relate $\|\mathbb{A}(\mu)-\tilde{\mathbb{A}}(\mu)\|_F^2$ to local errors $\|\mathbb{A}^i(\mu)-\tilde{\mathbb{A}}^i(\mu)\|_F^2$ and to subsequently invoke (4.7) to derive efficiently computable error bounds for $\|\mathbb{A}(\mu)-\tilde{\mathbb{A}}(\mu)\|_F^2$.

We start to analyze the contributions of $E_{\ell,\ell'}(\mu)$ and first note that an entry $E_{\ell,\ell'}(\mu)$ is nonzero only if the two GP degrees of freedom associated to ℓ and ℓ' have joint support. Moreover, we can group the SCS degrees of freedom in three sets based on the number of components on which the associated GPs have joint support: 1,2 or 4 components. We distinguish the following three cases (cf. Figure 6(a)):

1. Set $\mathcal{S}_1$: joint support on **one** component. This is the case for entries (ℓ,ℓ'), which are both associated to different line GPs, i.e., $\mathrm{GP}\neq\mathrm{GP}'$. In the previous example depicted in Fig. 7 there are no such global ports.

2. Set $\mathcal{S}_2$: joint support on **two** components. This is the case for entries (ℓ,ℓ'), which are both associated to the same line GP, i.e., $\mathrm{GP}=\mathrm{GP}'$, and for entries (ℓ,ℓ'), where one entry is associated to a line GP and the other entry is associated to a point GP. Referring to Fig. 7 such global ports are $\mathrm{GP},\mathrm{GP}'\in\{1,2,3,6,7,8\}$.

3. Set $\mathcal{S}_4$: joint support on **four** components. This is the case for entries (ℓ,ℓ'), which are both associated to point GPs and so $\ell=\ell'$. Referring to Fig. 7 such global ports are $\mathrm{GP}=\mathrm{GP}'\in\{4,5\}$.

We note that a finer distinction would be possible by explicitly accounting for line and point GPs on the boundary. However, the classification introduced above suffices for our purpose.

Since the union of the sets $\mathcal{S}_1$, $\mathcal{S}_2$, and $\mathcal{S}_4$ contains all possible interactions and thus nonzero entries of $E(\mu)$, we can write

$$\|E(\mu)\|_F^2 = \sum_{\ell,\ell'=1}^{n_{\mathbf{sc}}} E_{\ell,\ell'}(\mu)^2 = \sum_{\ell,\ell'\in\mathcal{S}_1} E_{\ell,\ell'}(\mu)^2 + \sum_{\ell,\ell'\in\mathcal{S}_2} E_{\ell,\ell'}(\mu)^2 + \sum_{\ell,\ell'\in\mathcal{S}_4} E_{\ell,\ell'}(\mu)^2. \tag{4.8}$$

We first focus on the set $\mathcal{S}_2$. We know that for $\ell,\ell'\in\mathcal{S}_2$ each entry of $\mathbb{A}(\mu)$ and $\tilde{\mathbb{A}}(\mu)$ is assembled from a sum of two local stiffness matrices. Let $\ell=(\mathrm{GP},k)$, we introduce — for notational convenience — the mapping $\mathcal{J}_i$ that maps $\ell=(\mathrm{GP},k)$ to the corresponding (LP,k) on component i (note that $\mathcal{J}_i$ is in fact already defined through the previously introduced mapping π resp. π_i^{-1}). We can thus write, for all $\ell,\ell'\in\mathcal{S}_2$,

$$\begin{aligned}
E_{\ell,\ell'}(\mu)^2 &= \big(\mathbb{A}_{\ell,\ell'}(\mu)-\tilde{\mathbb{A}}_{\ell,\ell'}(\mu)\big)^2 \\
&= \big(\mathbb{A}^{i_1}_{\mathcal{J}_{i_1}(\ell),\mathcal{J}_{i_1}(\ell')}(\mu)-\tilde{\mathbb{A}}^{i_1}_{\mathcal{J}_{i_1}(\ell),\mathcal{J}_{i_1}(\ell')}(\mu)+\mathbb{A}^{i_2}_{\mathcal{J}_{i_2}(\ell),\mathcal{J}_{i_2}(\ell')}(\mu)-\tilde{\mathbb{A}}^{i_2}_{\mathcal{J}_{i_2}(\ell),\mathcal{J}_{i_2}(\ell')}(\mu)\big)^2, \\
&\le 2\big(|\mathbb{A}^{i_1}_{\mathcal{J}_{i_1}(\ell),\mathcal{J}_{i_1}(\ell')}(\mu)-\tilde{\mathbb{A}}^{i_1}_{\mathcal{J}_{i_1}(\ell),\mathcal{J}_{i_1}(\ell')}(\mu)|^2+|\mathbb{A}^{i_2}_{\mathcal{J}_{i_2}(\ell),\mathcal{J}_{i_2}(\ell')}(\mu)-\tilde{\mathbb{A}}^{i_2}_{\mathcal{J}_{i_2}(\ell),\mathcal{J}_{i_2}(\ell')}(\mu)|^2\big) \\
&= 2\sum_{m=1}^{2}|\mathbb{A}^{i_m}_{\mathcal{J}_{i_m}(\ell),\mathcal{J}_{i_m}(\ell')}(\mu)-\tilde{\mathbb{A}}^{i_m}_{\mathcal{J}_{i_m}(\ell),\mathcal{J}_{i_m}(\ell')}(\mu)|^2,
\end{aligned} \tag{4.9}$$

where we used the inequality $(a+b)^2\le 2(a^2+b^2)$. We can proceed similarly for the set $\mathcal{S}_4$ by using the inequality $(a+b+c+d)^2\le 4(a^2+b^2+c^2+d^2)$ to bound the left hand side of (4.8) by

$$\begin{aligned}
\|\mathbb{A}(\mu)-\tilde{\mathbb{A}}(\mu)\|_F^2 \le & \sum_{\ell,\ell'\in\mathcal{S}_1}|\mathbb{A}^{i}_{\mathcal{J}_i(\ell),\mathcal{J}_i(\ell')}(\mu)-\tilde{\mathbb{A}}^{i}_{\mathcal{J}_i(\ell),\mathcal{J}_i(\ell')}(\mu)|^2 \\
&+2\sum_{\ell,\ell'\in\mathcal{S}_2}\sum_{m=1}^{2}|\mathbb{A}^{i_m}_{\mathcal{J}_{i_m}(\ell),\mathcal{J}_{i_m}(\ell')}(\mu)-\tilde{\mathbb{A}}^{i_m}_{\mathcal{J}_{i_m}(\ell),\mathcal{J}_{i_m}(\ell')}(\mu)|^2 \\
&+4\sum_{\ell,\ell'\in\mathcal{S}_4}\sum_{m=1}^{4}|\mathbb{A}^{i_m}_{\mathcal{J}_{i_m}(\ell),\mathcal{J}_{i_m}(\ell')}(\mu)-\tilde{\mathbb{A}}^{i_m}_{\mathcal{J}_{i_m}(\ell),\mathcal{J}_{i_m}(\ell')}(\mu)|^2.
\end{aligned} \tag{4.10}$$

It remains to bound the right hand side of (4.10) in terms of the *a posteriori* error bound introduced in the last section. We first note that we can bound the sum of the errors over all entries of the

component stiffness matrices and all components using (4.7) by

$$\begin{aligned}
&\sum_{\ell,\ell'\in\mathcal{S}_1} |\mathbb{A}^{i}_{\mathcal{J}_i(\ell),\mathcal{J}_i(\ell')}(\mu)-\tilde{\mathbb{A}}^{i}_{\mathcal{J}_i(\ell),\mathcal{J}_i(\ell')}(\mu)|^2 \\
&\quad +1\sum_{\ell,\ell'\in\mathcal{S}_2}\sum_{m=1}^{2} |\mathbb{A}^{i_m}_{\mathcal{J}_{i_m}(\ell),\mathcal{J}_{i_m}(\ell')}(\mu)-\tilde{\mathbb{A}}^{i_m}_{\mathcal{J}_{i_m}(\ell),\mathcal{J}_{i_m}(\ell')}(\mu)|^2 \\
&\quad\quad +1\sum_{\ell,\ell'\in\mathcal{S}_4}\sum_{m=1}^{4} |\mathbb{A}^{i_m}_{\mathcal{J}_{i_m}(\ell),\mathcal{J}_{i_m}(\ell')}(\mu)-\tilde{\mathbb{A}}^{i_m}_{\mathcal{J}_{i_m}(\ell),\mathcal{J}_{i_m}(\ell')}(\mu)|^2 \\
&\quad\quad = \sum_{i\in\mathcal{C}_{\mathrm{SYS}}} \|\mathbb{A}^{i}(\mu)-\tilde{\mathbb{A}}^{i}(\mu)\|_F^2 \overset{(4.7)}{\leq} \sum_{i\in\mathcal{C}_{\mathrm{SYS}}} \Big(\sum_{\mathrm{LP}\in\mathcal{P}_{\mathrm{COM}}}\sum_{k=1}^{n_{\pi(\mathrm{LP},i)}} \Delta_{\mathrm{LP},i,k}(\mu)^2\Big)^2. \qquad (4.11)
\end{aligned}$$

Second, recalling the definition of the set $\mathcal{S}_2$ we can bound the sum of the errors over $\mathcal{S}_2$ using

$$\begin{aligned}
\sum_{\ell,\ell'\in\mathcal{S}_2}\sum_{m=1}^{2} |\mathbb{A}^{i_m}_{\mathcal{J}_{i_m}(\ell),\mathcal{J}_{i_m}(\ell')}(\mu)-\tilde{\mathbb{A}}^{i_m}_{\mathcal{J}_{i_m}(\ell),\mathcal{J}_{i_m}(\ell')}(\mu)|^2 &\leq \sum_{i\in\mathcal{C}_{\mathrm{SYS}}}\sum_{\mathrm{LP}\in\mathcal{P}^l_{\mathrm{COM}}} \Big(\sum_{k=1}^{n_{\pi(\mathrm{LP},i)}} \Delta_{\mathrm{LP},i,k}(\mu)^2\Big)^2 \\
&\quad + \sum_{i\in\mathcal{C}_{\mathrm{SYS}}}\sum_{\mathrm{LP}\in\mathcal{P}^l_{\mathrm{COM}}}\sum_{k=1}^{n_{\pi(\mathrm{LP},i)}}\sum_{\mathrm{LP}'\in\mathcal{P}^c_{\mathrm{COM}}}\sum_{k'=1}^{n_{\pi(\mathrm{LP}',i)}} \big(\Delta_{\mathrm{LP},i,k}(\mu)\Delta_{\mathrm{LP}',i,k'}(\mu)\big)^2. \qquad (4.12)
\end{aligned}$$

Finally, since $\mathcal{S}_4$ contains only contributions from two point GPs (resp. LPs) we have similarly

$$\sum_{\ell,\ell'\in\mathcal{S}_4}\sum_{m=1}^{4} |\mathbb{A}^{i_m}_{\mathcal{J}_{i_m}(\ell),\mathcal{J}_{i_m}(\ell')}(\mu)-\tilde{\mathbb{A}}^{i_m}_{\mathcal{J}_{i_m}(\ell),\mathcal{J}_{i_m}(\ell')}(\mu)|^2 \leq \sum_{i\in\mathcal{C}_{\mathrm{SYS}}}\sum_{\mathrm{LP}\in\mathcal{P}^c_{\mathrm{COM}}}\sum_{k=1}^{n_{\pi(\mathrm{LP},i)}} \Delta_{\mathrm{LP},i,k}(\mu)^4. \qquad (4.13)$$

It thus follows from (4.10) by invoking (4.11), (4.12), and (4.13) that the error in the SCS stiffness matrix error is bounded by

$$\begin{aligned}
\|\mathbb{A}(\mu)-\tilde{\mathbb{A}}(\mu)\|_F^2 \leq \sum_{i\in\mathcal{C}_{\mathrm{SYS}}} \Big(\sum_{\mathrm{LP}\in\mathcal{P}_{\mathrm{COM}}}\sum_{k=1}^{n_{\pi(\mathrm{LP},i)}} \Delta_{\mathrm{LP},i,k}(\mu)^2\Big)^2 &+1\sum_{i\in\mathcal{C}_{\mathrm{SYS}}}\sum_{\mathrm{LP}\in\mathcal{P}^l_{\mathrm{COM}}} \Big(\sum_{k=1}^{n_{\pi(\mathrm{LP},i)}} \Delta_{\mathrm{LP},i,k}(\mu)^2\Big)^2 \\
&+1\sum_{i\in\mathcal{C}_{\mathrm{SYS}}}\sum_{\mathrm{LP}\in\mathcal{P}^l_{\mathrm{COM}}}\sum_{k=1}^{n_{\pi(\mathrm{LP},i)}}\sum_{\mathrm{LP}'\in\mathcal{P}^c_{\mathrm{COM}}}\sum_{k'=1}^{n_{\pi(\mathrm{LP}',i)}} \big(\Delta_{\mathrm{LP},i,k}(\mu)\Delta_{\mathrm{LP}',i,k'}(\mu)\big)^2 \\
&+3\sum_{i\in\mathcal{C}_{\mathrm{SYS}}}\sum_{\mathrm{LP}\in\mathcal{P}^c_{\mathrm{COM}}}\sum_{k=1}^{n_{\pi(\mathrm{LP},i)}} \Delta_{\mathrm{LP},i,k}(\mu)^4. \qquad (4.14)
\end{aligned}$$

We summarize this result in

Lemma 4.1. *For any $\mu\in\mathcal{D}$, the error in the right-hand side and the stiffness matrix of the Schur Complement System satisfies $\|\mathbb{F}(\mu)-\tilde{\mathbb{F}}(\mu)\|_2\leq\sigma_1(\mu)$ and $\|\mathbb{A}(\mu)-\tilde{\mathbb{A}}(\mu)\|_F\leq\sigma_2(\mu)$, where*

$$\sigma_1(\mu)^2 \equiv 2\sum_{i\in\mathcal{C}_{\mathrm{SYS}}} \Delta_{f,i}(\mu)^2 \left\{ \sum_{\mathrm{LP}\in\mathcal{P}^l_{\mathrm{COM}}}\sum_{k=1}^{n_{\pi(\mathrm{LP},i)}} \Delta_{\mathrm{LP},i,k}(\mu)^2 + 2\sum_{\mathrm{LP}\in\mathcal{P}^c_{\mathrm{COM}}}\sum_{k=1}^{n_{\pi(\mathrm{LP},i)}} \Delta_{\mathrm{LP},i,k}(\mu)^2 \right\}, \qquad (4.15)$$

and

$$\sigma_2(\mu)^2 \equiv \sum_{i\in\mathcal{C}_{\rm SYS}} \Bigg\{ \Big(\sum_{\rm LP\in\mathcal{P}_{\rm COM}} \sum_{k=1}^{n_{\pi({\rm LP},i)}} \Delta_{{\rm LP},i,k}(\mu)^2 \Big)^2 + \sum_{\rm LP\in\mathcal{P}^l_{\rm COM}} \Big(\sum_{k=1}^{n_{\pi({\rm LP},i)}} \Delta_{{\rm LP},i,k}(\mu)^2 \Big)^2 + \sum_{\rm LP\in\mathcal{P}^l_{\rm COM}} \sum_{k=1}^{n_{\pi({\rm LP},i)}} \sum_{{\rm LP}'\in\mathcal{P}^c_{\rm COM}} \sum_{k'=1}^{n_{\pi({\rm LP}',i)}} (\Delta_{{\rm LP},i,k}(\mu)\Delta_{{\rm LP}',i,k'}(\mu))^2 + 3 \sum_{\rm LP\in\mathcal{P}^c_{\rm COM}} \sum_{k=1}^{n_{\pi({\rm LP},i)}} \Delta_{{\rm LP},i,k}(\mu)^4 \Bigg\}. \tag{4.16}$$

Proof. The result (4.16) directly follows from our derivation leading up to (4.14). The proof for (4.15) follows similar arguments and is thus omitted. □

We next introduce the smallest eigenvalue $\tilde{\lambda}_{\min}(\mu) > 0$ of the reduced basis SCS stiffness matrix $\tilde{\mathbb{A}}(\mu)$. Following the idea presented in [12], Corollary 5.5, we propose an *a posteriori* error bound for $\|\mathbb{U}(\mu) - \tilde{\mathbb{U}}(\mu)\|_2$ in

Lemma 4.2. *We have* $\|(\mathbb{A}(\mu) - \tilde{\mathbb{A}}(\mu))\tilde{\mathbb{U}}(\mu)\|_2 \le \sigma_3(\mu)$, *where*

$$\begin{aligned}
\sigma_3(\mu)^2 \equiv & \sum_{i\in\mathcal{C}_{\rm SYS}} \Big(\sum_{\rm LP\in\mathcal{P}_{\rm COM}} \sum_{k=1}^{n_{\pi({\rm LP},i)}} \Delta_{{\rm LP},i,k}(\mu)^2 \Big) \Big(\sum_{\rm LP\in\mathcal{P}_{\rm COM}} \sum_{k=1}^{n_{\pi({\rm LP},i)}} \Delta_{{\rm LP},i,k}(\mu) |\tilde{\mathbb{U}}_{\mathcal{J}_i^{-1}({\rm LP},k)}(\mu)| \Big)^2 \\
& + \sum_{i\in\mathcal{C}_{\rm SYS}} \Big(\sum_{\rm LP\in\mathcal{P}^l_{\rm COM}} \sum_{k=1}^{n_{\pi({\rm LP},i)}} \Delta_{{\rm LP},i,k}(\mu)^2 \Big) \Big(\sum_{\rm LP\in\mathcal{P}^l_{\rm COM}} \sum_{k=1}^{n_{\pi({\rm LP},i)}} \Delta_{{\rm LP},i,k}(\mu) |\tilde{\mathbb{U}}_{\mathcal{J}_i^{-1}({\rm LP},k)}(\mu)| \Big)^2 \\
& + \sum_{i\in\mathcal{C}_{\rm SYS}} \Big(\sum_{\rm LP\in\mathcal{P}^l_{\rm COM}} \sum_{k=1}^{n_{\pi({\rm LP},i)}} \Delta_{{\rm LP},i,k}(\mu)^2 \Big) \Big(\sum_{\rm LP\in\mathcal{P}^c_{\rm COM}} \sum_{k=1}^{n_{\pi({\rm LP},i)}} (\Delta_{{\rm LP},i,k}(\mu) |\tilde{\mathbb{U}}_{\mathcal{J}_i^{-1}({\rm LP},k)}(\mu)|)^2 \Big) \\
& + 3 \sum_{i\in\mathcal{C}_{\rm SYS}} \sum_{\rm LP\in\mathcal{P}^c_{\rm COM}} \sum_{k=1}^{n_{\pi({\rm LP},i)}} \Delta_{{\rm LP},i,k}(\mu)^2 (\Delta_{{\rm LP},i,k}(\mu) |\tilde{\mathbb{U}}_{\mathcal{J}_i^{-1}({\rm LP},k)}(\mu)|)^2,
\end{aligned} \tag{4.17}$$

and the inverse operator $\mathcal{J}_i^{-1}$ *maps an* LP *degree of freedom* $({\rm LP},k)$ *of component* i *to a global entry in the SCS solution* $\ell = ({\rm GP},k)$.

Proof. The first part of the proof, i.e., obtaining a bound for $\|(\mathbb{A}^i(\mu) - \tilde{\mathbb{A}}^i(\mu))\tilde{\mathbb{U}}^i(\mu)\|_2^2$, follows directly from the proof of Corollary 5.5 in [12]. However, when summing up the contributions over all components $i \in \mathcal{C}_{\rm SYS}$, we again consider the set $\mathcal{S}_1$, $\mathcal{S}_2$, and $\mathcal{S}_4$ separately and bound the terms following the ideas in (4.10)–(4.14) to arrive at (4.17). □

Finally, we obtain the bound for the system level error in

Proposition 4.1. If $\tilde{\lambda}_{\min}(\mu) - \sigma_2(\mu) > 0$, the error, $\|\mathbb{U}(\mu) - \tilde{\mathbb{U}}(\mu)\|_2$, satisfies for all $\mu \in \mathcal{D}$

$$\|\mathbb{U}(\mu) - \tilde{\mathbb{U}}(\mu)\|_2 \le \Delta^{\mathbb{U}}(\mu) \equiv \frac{\sigma_1(\mu) + \sigma_3(\mu) + \|\tilde{\mathbb{F}}(\mu) - \tilde{\mathbb{A}}(\mu)\tilde{\mathbb{U}}(\mu)\|_2}{\tilde{\lambda}_{\min}(\mu) - \sigma_2(\mu)}. \tag{4.18}$$

Proof. The proof follows directly from the proof of Proposition 4.3 in [12] and invoking Lemma 4.1 and 4.2. □

Remark 4.1. We can obtain a much simpler but slightly more conservative bound for $\|\mathbb{A}(\mu)-\tilde{\mathbb{A}}(\mu)\|_F$ by assuming that a component always has the maximum possible number of neighbors per port. Since an interior point GP is connected to four components, we directly obtain the bound

$$\|\mathbb{A}(\mu)-\tilde{\mathbb{A}}(\mu)\|_F \leq \left\{ 4 \sum_{i\in\mathcal{C}_{\mathrm{SYS}}} \left(\sum_{\mathrm{LP}\in\mathcal{P}_{\mathrm{COM}}} \sum_{k=1}^{n_{\pi(\mathrm{LP},i)}} \Delta_{\mathrm{LP},i,k}(\mu)^2 \right)^2 \right\}^{1/2} \tag{4.19}$$

instead of (4.16).

5 Numerical Results

We return to our application introduced in Section 2. We consider the unfolded bearing sketched in Figure 2, which is composed of 18×4 similar components Ω_i; we thus have 72 components. We recall the governing equation (2.7) and the input parameter $\mu=\{u_1,h_0,h_x,h_{\mathrm{gr}}\}\in\mathcal{D}\subset\mathbb{R}^4$, where the parameter domain is given by $\mathcal{D}=[12\mathrm{m/s},13\mathrm{m/s}]\times[10^{-5}\mathrm{m},5\times10^{-5}\mathrm{m}]\times[-4\times10^{-5},4\times10^{-5}]\times[0.5\times10^{-5}\mathrm{m},1.5\times10^{-5}\mathrm{m}]$ with the additional constraint that $h_0+h_x\frac{x}{\Delta x}\in[10^{-5}\mathrm{m},5\times10^{-5}\mathrm{m}]$, where $x\in[0,\Delta x]$ and Δx is the component size in the x-direction, see Fig. 2. For completeness we note that x is shifted by $x-k\cdot\Delta x$, $k=0,\ldots,17$ according to the position of the component. The dynamic viscosity is set to $\mu_V=0.01\mathrm{Pa\cdot s}$ for all results. We next consider a single component with the groove in the middle sketched in Figure 4 and introduce a piecewise linear finite element approximation subspace of dimension $\dim(X_i)=480$.

In the offline stage, we first compute the eigenmodes and their harmonic extensions following the procedure outlined in Section 3.2.1. The reduced basis spaces $\tilde{X}_{f,i;0}$ and $\tilde{X}_{\mathrm{LP},i,k;0}$ for the bubble functions introduced in Section 3.2.2 are constructed using a Greedy procedure [24]. To this end, we introduce a regular $7\times5\times9\times4$ train sample Ξ_{train} of size $n_{\mathrm{train}}=1568$ (we exclude parameters in the training set where the constraint on $h_0+h_x\frac{x}{\Delta x}$ is not fulfilled) and stop the Greedy procedure when the desired relative error tolerance $\varepsilon_{\mathrm{rel}}^{\mathrm{en}}=1\mathrm{E}{-2}$ is reached.

We next turn to the online stage and consider the specific parameter value $u_1=4\pi\mathrm{m/s}$ and $h_{\mathrm{gr}}=10^{-5}\mathrm{m}$. Note that the parameters h_0 and h_x change for each component along the circumference of the bearing to model the gap height sketched in Figure 1(b). In Figure 8(a) and (b) we plot the solution of the reduced basis SCS projected onto the (system level) finite element space X and the error between the reduced basis SCS solution and a finite element (system level) solution (i.e., on the space X), respectively. We observe that the SCRBE solution is very close to the finite element solution: the relative L^∞-norm of the error is $1.6\mathrm{E}{-4}$ and the relative H^1-norm $6.2\mathrm{E}{-5}$. We also observe from Figure 8(a) that the influence of the grooves on the pressure is clearly visible

To assess the overall quality of the SCRBE solution and SCRBE error bounds, we introduce a regular test sample Ξ_{test} of size $n_{\mathrm{test}}=99$. For the test sample, we also consider different gap heights by varying the amplitude and the eccentricity of the bearing. We again first compare the SCRBE solution to a finite element solution: the maximum relative L^∞ error over Ξ_{test} is $2.4\mathrm{E}{-4}$

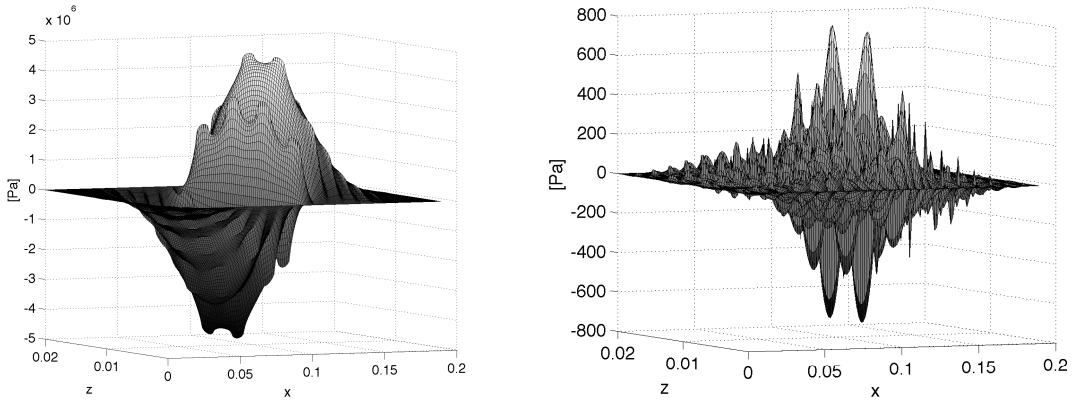

(a) (b)

Figure 8: (a) SCRBE solution and (b) error between finite element and SCRBE solution.

and the maximum relative H^1 error is $6.9\mathrm{E}{-5}$ showing that the reduced basis SCS solution is very accurate over the parameter domain. We next compute the maximum absolute and relative system level *a posteriori* error bound (4.18) presented in Table 2. We also compute an *a posteriori* error bound following Remark 4.1, i.e., bounding the Frobenius norm error of the component stiffness matrices by assuming the maximum number of neighbors for all ports. This bound is denoted with a hat and presented in the right two columns of Table 2. We observe that we obtain a very good accuracy for both bounds and that the latter bound is approximately 50% larger than the more elaborate bound.

$\Delta^{\mathbb{U}}_{\max}$	$\Delta^{\mathbb{U}}_{\max}/\|\tilde{\mathbb{U}}(\mu)\|_2$	$\hat{\Delta}^{\mathbb{U}}_{\max}$	$\hat{\Delta}^{\mathbb{U}}_{\max}/\|\tilde{\mathbb{U}}(\mu)\|_2$
$1.1\mathrm{E}{+4}$	$8.3\mathrm{E}{-4}$	$1.7\mathrm{E}{+4}$	$1.3\mathrm{E}{-3}$

Table 2: Maximum absolute and maximum relative error bound over Ξ_{test}.

We finally comment on the computational times. The offline stage for the SCRBE method requires 3050s, the online solution including the computation of the *a posteriori* error bound takes 5.5s (assembly $\approx$3s, SCS-solve $\approx$0.07s, and bound computation $\approx$2s)[§]. In contrast, the assembly and solution of the finite element approximation requires approximately 14s resulting in an overall speed-up of ≈ 3. However, this is not surprising given the fairly small dimension of our model problem. In fact, we expect that the efficiency of the method improves considerably as the ratio of the "internal", i.e., statically condensed, degrees of freedom to the port degrees of freedom increases.

[§]All computations are performed on an Intel® i5 with MATLAB® 7.13

6 Conclusions

We presented a static condensation reduced basis element method for problems where the domain decomposition results in several components being connected at a single port, a typical example being a checkerboard pattern. Although our work was motivated by the Reynolds Lubrication equation governing the pressure distribution in a plain bearing, the methodology directly extends to other physical problem requiring a similar domain decomposition.

For this case, we proposed a new eigenfunction expansion to represent the port degrees of freedom. Here, we had to distinguish between ports represented by lines and corners, and also guarantee consistent boundary conditions for the harmonic extension of the eigenfunctions into the component domain. Furthermore, we derived a system level *a posteriori* error bound, which takes the number of components connected at each port explicitly into account.

It turns out that the efficiency of the method strongly depends on the ratio between the internal and port degrees of freedom of the components. In this sense, the checkerboard pattern considered in this paper admittedly presents a "difficult" problem in terms of computational gain. However, the extension of the static condensation reduced basis element method to such problems also allows for a wider applicability in the engineering context.

Acknowledgments

We would like to thank Prof. A.T. Patera and Dr. J. Eftang for helpful discussions on the SCRBE method as well as Prof. G. Knoll and Dr. R. Schönen from ISTmbH for providing the specific application. This work was supported by the Excellence Initiative of the German federal and state governments and the German Research Foundation through Grant GSC 111.

References

[1] E. Bader. A reduced basis element approach for the reynolds lubrication equation. Master's thesis, RWTH Aachen University, 2012.

[2] S. Bai, X. Peng, Y. Li, and S. Sheng. A hydrodynamic laser surface-textured gas mechanical face seal. *Tribology Letters*, 38(2):187–194, 2010.

[3] B. Bhushan. *Principle and Applications of Tribology, 2nd Edition*. Tribology Series. Wiley, 2013.

[4] T. F. Chan and T. P. Mathew. Domain decomposition algorithms. *Acta Numerica*, 3:61–143, 1 1994.

[5] R. R. Craig Jr. and M. C. Bampton. Coupling of substructures for dynami analyses. *AIAA Journal*, 6(7):1313–1319, 1968.

[6] J. L. Eftang, D. B. P. Huynh, D. J. Knezevic, E. M. Rønquist, and A. T. Patera. Adaptive port reduction in static condensation. In *Proceedings of 7th Vienna Conference on Mathematical Modelling (MATHMOD 2012)*, 2012.

[7] J. L. Eftang and A. T. Patera. Port reduction in parametrized component static condensation: approximation and a posteriori error estimation. *Int. J. Numer. Methods Eng.*, 96(5):269–302, 2013.

[8] G. B. Gadeschi, K. Backhaus, and G. Knoll. Numerical analysis of laser-textured piston-rings in the hydrodynamic lubrication regime. *Journal of Tribology*, 134(4):8 pages, 2012.

[9] J. S. Hesthaven, G. Rozza, and B. Stamm. *Certified Reduced Basis Methods for Parametrized Partial Differential Equations*. SpringerBriefs in Mathematics, 2015.

[10] W. C. Hurty. Dynamic analysis of structural systems using component modes. *AIAA Journal*, 3(4):678–685, 1965.

[11] D. B. P. Huynh. A static condensation reduced basis element approximation: Application to three-dimensional acoustic muffler analysis. *International Journal of Computational Methods*, 11(03):1343010, 2014.

[12] D. B. P. Huynh, D. J. Knezevic, and A. T. Patera. A static condensation reduced basis element method: approximation and a posteriori error estimation. *ESAIM: Math. Model. Num.*, 47:213–251, 1 2013.

[13] D. B. P. Huynh, D. J. Knezevic, and A. T. Patera. A static condensation reduced basis element method: complex problems. *Comput. Methods Appl. Mech. Engrg.*, 259(0):197–216, 2013.

[14] D. B. P. Huynh, G. Rozza, S. Sen, and A. T. Patera. A successive constraint linear optimization method for lower bounds of parametric coercivity and inf-sup stability constants. *C. R. Math.*, 345(8):473–478, 2007.

[15] S. Kango, D. Singh, and R. Sharma. Numerical investigation on the influence of surface texture on the performance of hydrodynamic journal bearing. *Meccanica*, 47(2):469–482, 2012.

[16] K. Kumar Gupta, R. Kumar, H. Kumar, and M. Sharma. Study on effect of surface texture on the performance of hydrodynamic journal bearing. *International Journal of Engineering and Advanced Technology*, 3(1):49–54, 2013.

[17] Y. Maday and E. M. Rønquist. A reduced-basis element method. *J. Sci. Comput.*, 17:447–459, 2002. 10.1023/A:1015197908587.

[18] Y. Maday and E. M. Rønquist. The reduced basis element method: Application to a thermal fin problem. *SIAM J. Sci. Comput.*, 26(1):240–258, 2004.

[19] K. Murty. Note on a bard-type scheme for solving the complementarity problem. *Opsearch*, 11:123–130, 1974.

[20] O. Pinkus and B. Sternlicht. *Theory of hydrodynamic lubrication*. McGraw-Hill, 1961.

[21] C. Prud'homme, D. V. Rovas, K. Veroy, L. Machiels, Y. Maday, A. T. Patera, and G. Turinici. Reliable real-time solution of parametrized partial differential equations: Reduced-basis output bound methods. *J. Fluid. Eng.*, 124(1):70–80, 2002.

[22] G. Rozza, D. Huynh, and A. Patera. Reduced basis approximation and a posteriori error estimation for affinely parametrized elliptic coercive partial differential equations. *Archives of Computational Methods in Engineering*, 15(3):229–275, 2008.

[23] S. Vallaghé and A. Patera. The static condensation reduced basis element method for a mixed-mean conjugate heat exchanger model. *SIAM J. Sci. Comput.*, 36(3):B294–B320, 2014.

[24] K. Veroy, C. Prud'homme, D. V. Rovas, and A. T. Patera. A posteriori error bounds for reduced-basis approximation of parametrized noncoercive and nonlinear elliptic partial differential equations. In *Proceedings of the 16th AIAA Computational Fluid Dynamics Conference*, 2003. AIAA Paper 2003-3847.